VOL. 11, NO. 20, OCTOBER 2016 ISSN 1819-6608
ARPN Journal of Engineering and Applied Sciences


www.arpnjournals.com

DISCRIMINATION OF EXUDATES AND NON EXUDATES PIXELS IN FUNDUS IMAGES AND CLASSIFICATION OF COLOR AUTOCORRELOGRAM FEATURES USING MULTILAYER PERCEPTRON AND SUPPORT VECTOR MACHINE

Hasliza Abu Hassan[1,2], Nooritawati Md Tahir[1], Ahmad Ihsan Yassin[1] and Azlee Zabidi[1]
[1]Faculty of Electrical Engineering, Universiti Teknologi Mara, Shah Alam, Selangor, Malaysia
[2]Department Electrical Engineering, Faculty of Engineering, Universiti Selangor, Bestari Jaya, Selangor, Malaysia
E-Mail: ellyza90210@yahoo.com

ABSTRACT

Fundus images provide an opportunity for early detection of diabetes. Generally, retina fundus images of diabetic patients exhibit exudates, which are lesions indicative of Diabetic Retinopathy (DR). Computational tools have the potential to assist medical practitioners in early screening of the disease. The experiment consists of two parts: 1) detection of exudates in the fundus image (using the Multilayer Perceptron (MLP1) and Support Vector Machine (SVM1)), followed by 2) removal of exudates detected in step (1), feature representation using Color Autocorrelogram (CAC) and classification using another set of classifiers (MLP2 and SVM2). Experimental results on the MESSIDOR dataset suggest that the method has the potential to be used for early indication of DR.

Keywords: diabetic retinopathy, optic disc, multilayer perceptron, support vector machine, color autocorrelogram.

INTRODUCTION

Diabetes mellitus affects ten of million people around the world, and statistics indicate that this number will double in the future[1]. According to [2], 3.3 million cases of diabetes were in Malaysia in 2015 alone. The disease is divided into two categories namely Type I (insulin-dependent) and Type II (insulin-independent) [3, 4]. Among the symptoms of diabetes are delayed wound healing, infections of the urinary system, numbness, thirst, frequent urination and fatigue as well as weight loss. Due to the generic nature of the symptoms, the disease has a tendency to be detected only in advanced stages[4].

One of the symptoms of diabetes is DR which causes abnormalities in the retina such as micro aneurysms, exudates, macular edema, haemorrhages and neovascularization [5] leading to blindness if left untreated [6]. However, most diabetic patients have no awareness of the importance of eye checkups[7].

A fundus image is an of the eye's interior surface, which includes the retina, optic disc, macula, fovea and posterior pole [8, 9]. This fundus image provides an opportunity for early detection of diabetes with the assistance of modern computational methods. Retina fundus images of diabetic patients exhibit exudates, which are lesions indicative of DR.

Recent works on diagnosis of disease using fundus

Several recent works focusing on fundus analysis to detect diseases has been reported in [10-19]. In [10], fundus images were used to diagnose three stages of Diabetic Macular Edema (DME). Features extracted using the marker controlled watershed method was classified automatically using the Early Treatment Diabetic Retinopathy Study (ETDRS) grading scale.

In [20] presented an automated detection method for exudates and Optical Disc (OD) in retinal images using curvelet transform. The proposed exudates detection method consisted of steps such as creating the mask image, contrast enhancement and extraction of yellowish candidate features. For yellowish candidate features extraction, curvelet coefficients were used to modify bright lesions in the fundus image. The detection sensitivity and specificity were 98.4% and 90.1% respectively.

In [21] proposed a method to detect hard exudates from diabetic retinopathy images using fuzzy logic. In this method, the elimination of OD was done prior to further analysis to remove it from detection. The hard exudates were then classified using fuzzy logic. The fuzzy output was calculated for all the pixels according to a ratio of the hard exudates area. The results found the sensitivity and specificity of detecting hard exudates as 75.43% and 99.99% respectively. A similar method was presented in [24] where a Fuzzy Clustering Method (FCM) was used to classify the pixels in the fundus images with sensitivity, specificity and accuracy of 91.11%, 97.95% and 97.67% respectively.

In[16], binary masking was used as a pre-processing method for separating noise from fundus images. Local mean and variance-based method were used for background extraction. The proposed method showed good separation of noise from the original fundus image. Similarly, in[17] used the branch filtering approach to detect retinal blood vessels in fundus images.

In [22] used Artificial Neural Network (ANN) and Support Vector Machine (SVM) for exudates classification. Color spaces such as RGB, HIS, LAB and LUV were used to separate luminance and chrominance values from the images. Then, the segmented exudates lesions were classified using ANN and SVM. Using ANN, the sensitivity and specificity were 95.0% and 88.9% respectively. In comparison, SVM obtained 87.5%

sensitivity and 92.0% specificity for abnormal and normal cases. Similarly, in [25] used the ANN classifier with sensitivity of 96.97%, specificity of 100% and classification accuracy of 98.45%.

In [23], a combination of intensity thresholding and morphological techniques were used to detect exudates. Since the green channel of the Red, Green, Blue (RGB) image representation contains the highest information contents, information from the green channel was dilated twice with different structuring elements to generate a ring filter to extract the exudates.

Recent works involving color autocorrelogram (CAC)

In [30]proposed a new color feature descriptor called Color Mutual Information (CMI) to reduce computational complexity and low retrieval accuracy. To reduce computational complexity, the average mutual information between one color and all the colors surrounding it in the correlation feature matrix was calculated to obtain the new color feature vector. Then, inter-feature normalization was applied in combination of CMI and CAC (CAMI) to increase retrieval accuracy.

In [34], HSV, CAC and color moments were used for color feature analysis, while Gabor wavelets were used for texture feature analysis. In [35], the CAC was modified to extract features for detection of microaneurysm and neovascularisation.

Color autocorrelogram (CAC)

The CAC terms is introduced by Huang in late 90s [26]. In his work, he discovered a significant difference in the CAC when there is a change in spatial layout compared to color histograms [26, 27]. The work was an attempt to improve on the color histogram technique, which does not include any spatial information and captures only the color distribution in the image [28].

Several approaches have been explored in the combination of color with spatial information [29-32]. The spatial correlation of color pairs that changes with distance is called color correlogram [27]. Meanwhile, a subset of color correlogram, which measures the spatial correlation between identical colors is CAC [27, 33]. CAC eliminates the need for expensive memory cost and computational time using color correlogram [31].

The CAC of image (I) captures the spatial correlation between identical colors only and is defined by:

$$\alpha_c^{(d)}(I) = \gamma_{c,c}^{(d)}(I) \quad (1)$$

The probability of finding the same color at exactly distance (d)away was computed for each color distance pair (c,d).

METHODOLOGY

A total of 149 fundus images from the publicly available MESSIDOR databases were used to test the proposed method. The images were acquired using a color video 3CCD camera on a Topcon TRC NW6 non-mydriatic retinograph with a 45 degree field of view [36]. The proposed flowcharts are shown in Figure-2 and Figure-3.

Several pre-processing steps were performed to normalize the appearance of the fundus images, as well as removes the OD that may interfere with the classification process. The experiment was to design and implement two classifiers (MLP1 and SVM1) for feature extraction to classify exudates and non-exudates pixels. This was done by collecting samples of exudates and non-exudates pixels to train the MLP1 and SVM1 classifiers subject to different parameters, such as hidden units and kernel functions. After training was completed, the classifiers were both applied to six test images to determine the best classifier and optimal parameters for it.

Following that, the optimal parameters were used to detect exudates present in 149 fundus images (after pre-processing). Then, the CAC results have been verified using MLP2 and SVM2 to classify accuracy.

Pre-processing: Image normalization and removal of OD

The first step in our approach is to normalize the images using the histogram equalization method. This is done by first examining the color histogram of the image, then using the histogram to help balance the intensities of the colors in the image based on a predefined reference image (I_{ref}) as shown in Figure-5 (i). This is to ensure that all the images in the dataset are consistent prior to OD removal. The normalized images are referred to as I_{norm}.

Since the OD has characteristics similar to the exudates, they may be falsely classified as lesions [37]. Therefore, removal of the OD from I_{norm} would improve the classification of the remaining exudates regions [38]. The OD is excluded from all images by marking the center of the OD region in I_{norm} and expanding the circle radius manually until the entire OD has been covered. For convenience, images with removed OD are referred to as I_{wod}.

Discrimination of exudates and non-exudates pixels using MLP1 and SVM1

This step is concerned with constructing an optimal classifier to discriminate between exudate and non-exudate pixels based on their RGB color characteristics. To achieve this, samples of exudate, non-exudate and the background pixel region were obtained from several randomly selected fundus images. A total of 4,830 pixels were chosen manually from the selected fundus images as training data for the MLP1 and SVM1. From that number, 2,696 pixels represented exudates while 2,134 pixels represented non-exudates and background. The six selected fundus images are shown in Figure-1.These images were used to assist in the search for optimal parameters for the classifiers.

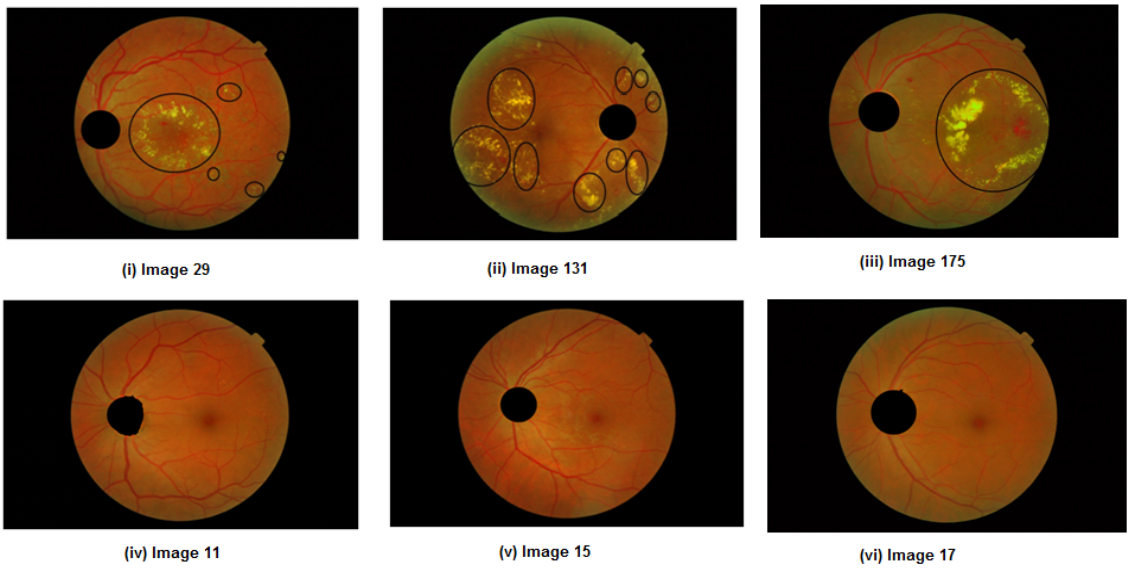

Figure-1. Six fundus images (3 exudates, 3 normal).

MLP1 implementation

For MLP1 training, a three-layer feed-forward structure was used. The input layer was fed with RGB pixel values. While for the hidden layer, the numbers of hidden units were varied between 1 and 5. The output layer was trained to output a binary decision (1 for exudate, 0 for non-exudate / background). The tangent-sigmoid activation function was used in the hidden and output layers as this structure is most suited for pattern classification problem. The Scaled Conjugate Gradient (SCG) algorithm was used as the training algorithm due to its excellent performance in pattern classification problems [39]. Table-1 shows the MLP1 parameter settings used.

Table-1.MLP1 structure and parameter settings.

Parameter	Setting
Structure	3-layer MLP1 with varied hidden unit
Activation function	Tangent-sigmoid at hidden and output layers
Training algorithm	SCG
Maximum epoch	200
Objective criterion	Mean Squared Error
Division of training, validation and testing set (%)	70:15:15

SVM1 implementation

Similar to MLP1, the SVM was trained using samples of exudate and non-exudate pixels. Several kernel structures were tested: linear, polynomial, quadratic and Radial Basis Function (RBF). The inputs for the SVM1 are the RGB values of each pixel. The SVM1 generated a binary output that indicates whether the pixel under examination is exudate or vice versa. Theoretically, SVM is developed based on the statistical learning theory and Vapnik-Chervonenkis (VC) dimension[40]. The regularization parameter (C) is equal to 1. The best model of SVM1 depends on the number of support vectors, C and kernel function parameter. The smallest number of support vector indicates good classifier, which is least number of the difficult data point[40]. Table-2 shows the SVM1 structure and parameter settings used.

Table-2.SVM1structure and parameter settings.

Parameter	Setting
Kernel function	Linear, polynomial, quadratic and RBF
Regularization parameter	C = 1
Division training and testing set (%)	50 : 50

CAC implementation

The CAC method needs to go through all the neighbors for each pixel in the image. It is an extension of the color histogram that adds a dimension to the feature vector, which represents the relative local distance k between pixels with the specific color [32]. Visualization was performed by extracting CAC features from I_{wod} and invert mask I_{wl}.

The CAC method needs to go through all the neighbors for each pixel in the image. It is an extension of the color histogram that adds a dimension to the feature vector, which represents the relative local distance k between pixels with the specific color [32].

The inputs for the CAC are image in unsigned 8 bit integers (uint8) form which representing the color image and distance vector that representing the different distances, in which the color distribution is calculated. The output for the CAC is the correlogram vector, which is a straight vector representing the probabilities of occurrence of 64 quantized colors. Its total dimension is 64n x 1 where n is the number of different distances.

Classification of CAC features using MLP2

For MLP2 training, a three-layer feed-forward structure was used. The input layer was fed with the subtraction of values from invert mask I_{wl} minus I_{wod} fundus images. While for the hidden layer, the numbers of hidden units were varied between 2, 4, 6, 8 and 10. The output layer was trained to output a binary decision (1 for DR condition, 0 for normal). The tangent-sigmoid activation function was used in the hidden and output layers. The Scaled Conjugate Gradient (SCG) algorithm was used as the training algorithm. The training, validation and testing were set to 70:15:15.

Classification of CAC features using SVM2

The SVM2 was trained using input similar to MLP2. Several kernel structures were tested: linear, polynomial, quadratic and RBF. The SVM2 generated a binary output that indicates whether the CAC features under examination is DR condition or vice versa. Regularization parameter (C) is equal to 1. The division between training and testing was set to 50:50. The best model of SVM depends on support vector, C and kernel function parameters.

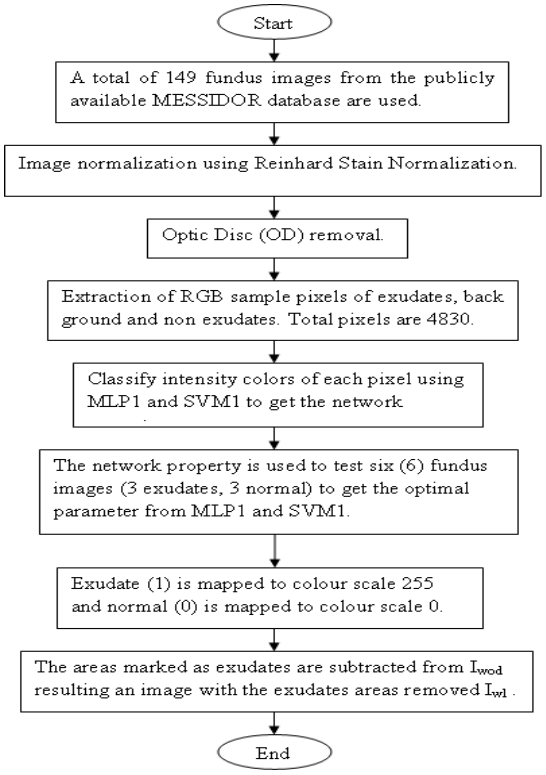

Figure-2. Experiment I: Determination of optimal parameter using MLP1 and SVM1.

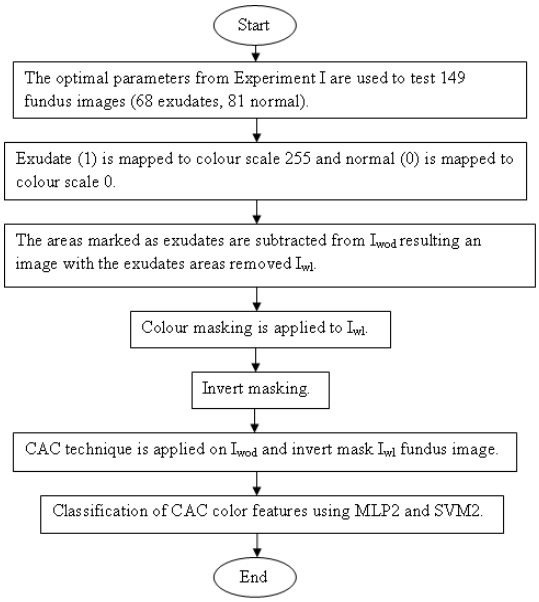

Figure-3. Experiment II: Visualization of exudates using CAC and classified using MLP2 and SVM2.

RESULTS AND DISCUSSION

Experimental analysis and testing are running on a Toshiba Satellite laptop Intel Core i7 Central Processing Unit (CPU), 2.1 (GHz) with 4 GB of Random Access Memory (RAM). Window 7 was installed as the operating

system. All programs were implemented using MATLAB version 8.1.0.604.

Image normalization and removal of OD

The normalization and removal of OD results are presented. Figure-4 shows the color histogram for the reference image (I_{ref}), the target image before normalization and the target image after Reinhard-Stain normalization. As can be seen, the histogram of the original image has been adjusted to approximate the reference image after the normalization process. The change in histogram distribution reflects that the color spectrum of the original image has been standardized to follow the reference (Figure-5). Figure-5(iii) shows the final step of OD removal from I_{norm}. Both normalization and OD removal were applied to all images in the dataset.

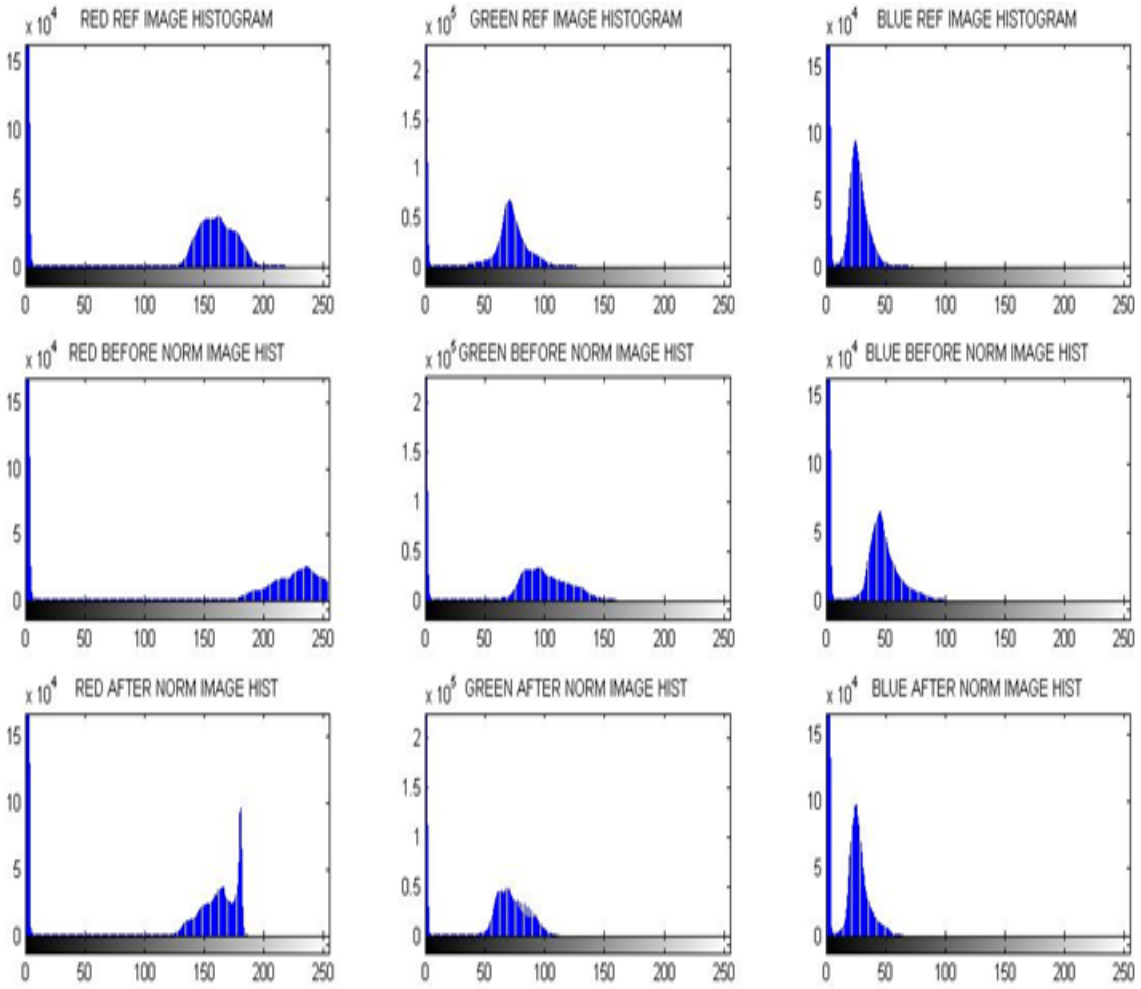

Figure-4. Color histogram before and after normalization of fundus images.

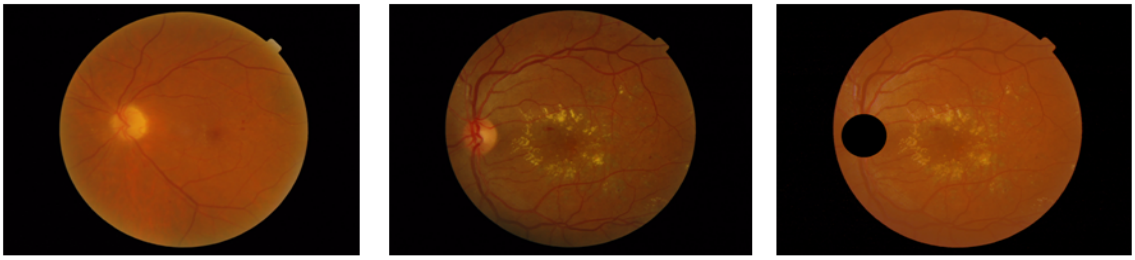

(i) **(ii)** **(iii)**

Figure-5.(i) Reference image (I_{ref}), (ii) Before normalization and (iii) After normalization with removal OD fundus image.

Results of MLP1 and SVM1

The MLP1 and SVM1 classifiers were both applied to six test images to determine the best optimal parameters for it. A summary of classification results for MLP1 and SVM1 is shown in Table-3 and Table-4.

Sample classification results for MLP1 (Figure-6 Figure-11) and SVM1 (Figure-12-Figure-17) are shown for I_{wod} in Figure-1(i) until Figure-1 (vi). As can be seen, the hidden units and kernel function settings have an effect on the classification results. For MLP1, it was observed that the best parameter in classifying pixels is hidden unit 2 because it can extract exudates and non-exudate candidates efficiently. Even though hidden unit 3, 4 and 5 show perfect classification accuracy in Table-3, the classification results were found to over-fit because it cannot discriminate between exudate and non-exudate pixels effectively(Figure-6 until Figure-11) albeit the high classification results in the testing set.

A similar observation was discovered for SVM1. The best kernel function for classifying the pixels was the linear kernel. Despite the fact that polynomial, quadratic and RBF kernel functions show precise accuracy on the training set in Table-4, they were over-fitted because it cannot extract exudates pixels efficiently on the actual fundus image (Figure-12-Figure-17).

Table-3. MLP1 hidden unit and pixels classifications.

Hidden Unit	Classification Accuracy
1	Training = 56.2% Testing = 53.2%
2	Training = 96.4% Testing = 96.4%
3	Training = 96.6% Testing = 95.7%
4	Training =100% Testing = 100%
5	Training = 100% Testing = 100%

Table-4.SVM1 kernel functions and pixels classifications.

Kernel Function	Classification Accuracy
Linear	Training = 97.0% Testing = 95.9%
Polynomial	Training = 100% Testing = 100%
Quadratic	Training = 99.6% Testing = 99.6%
RBF	Training = 99.3% Testing = 99.1%

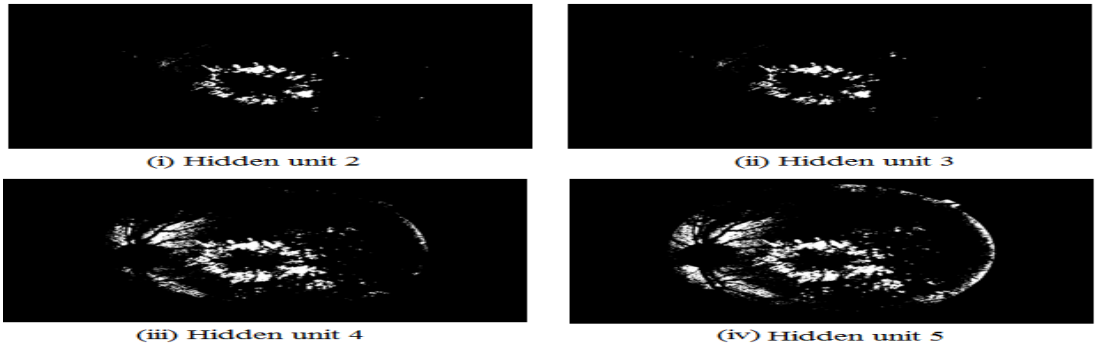

Figure-6. Black and white masking image of Figure-1 (i) with varied hidden units.

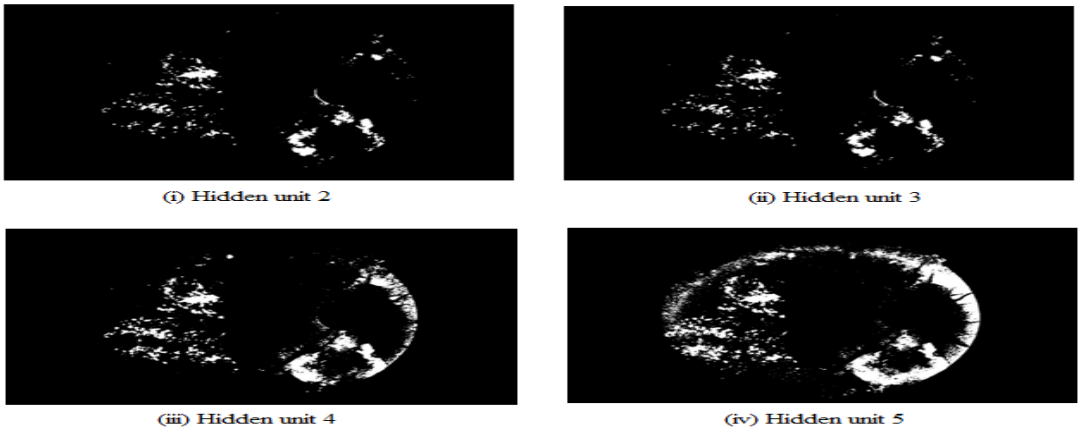

Figure-7. Black and white masking image of Figure-1 (ii) with varied hidden units.

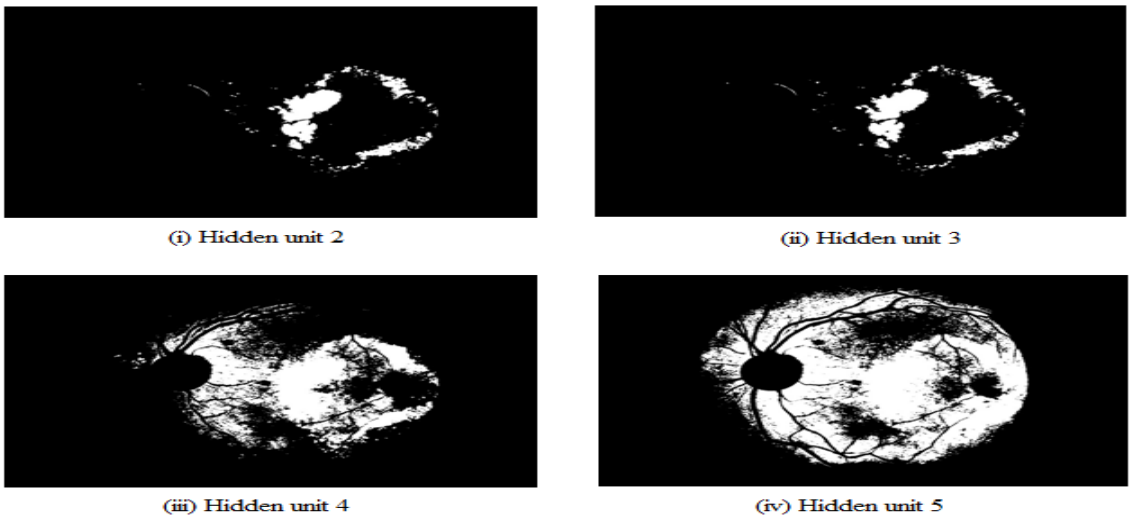

Figure-8. Black and white masking image of Figure-1(iii) with varied hidden units.

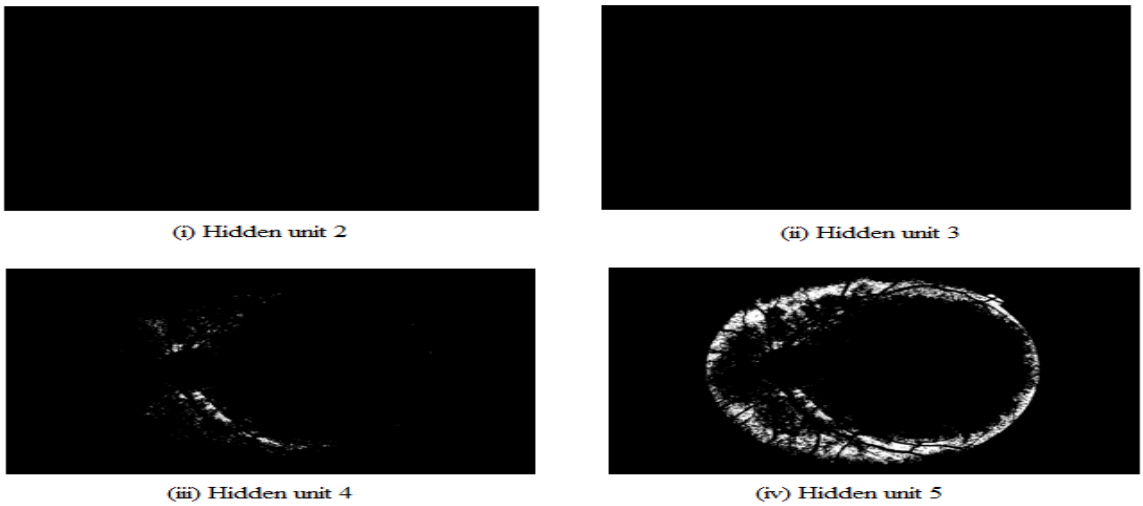

Figure-9. Black and white masking image of Figure-1 (iv) with varied hidden units.

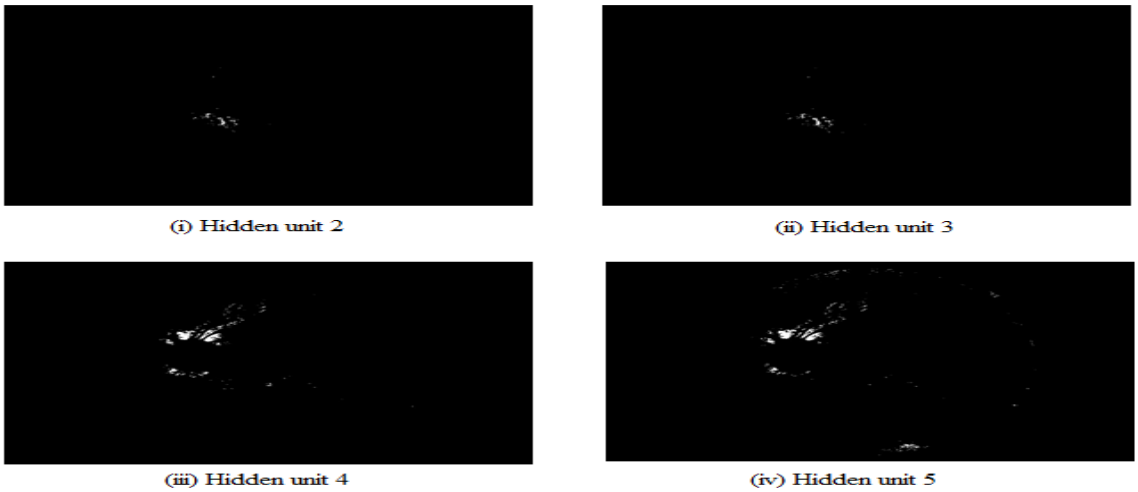

Figure-10. Black and white masking image of Figure-1(v) with varied hidden units.

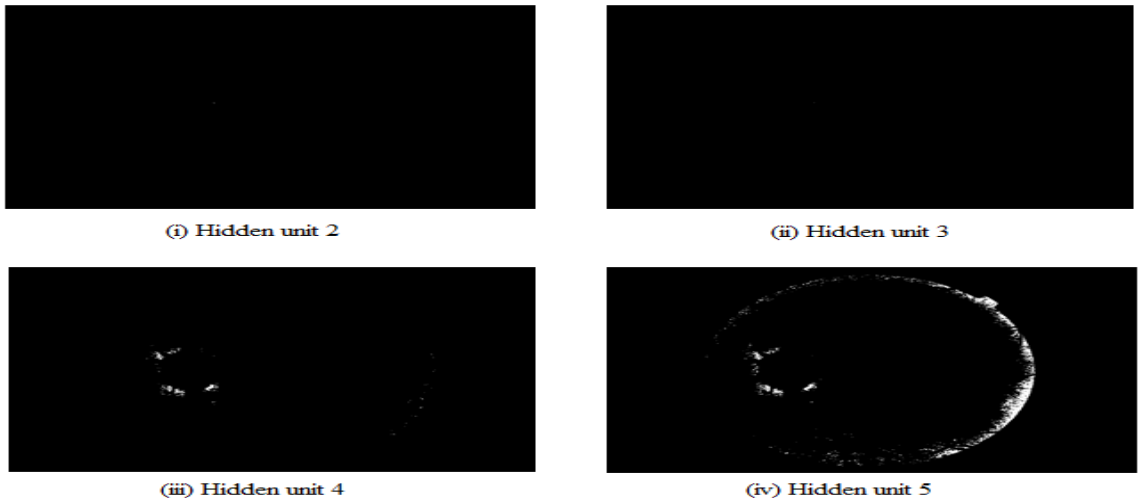

Figure-11. Black and white masking image of Figure-1(vi) with varied hidden units.

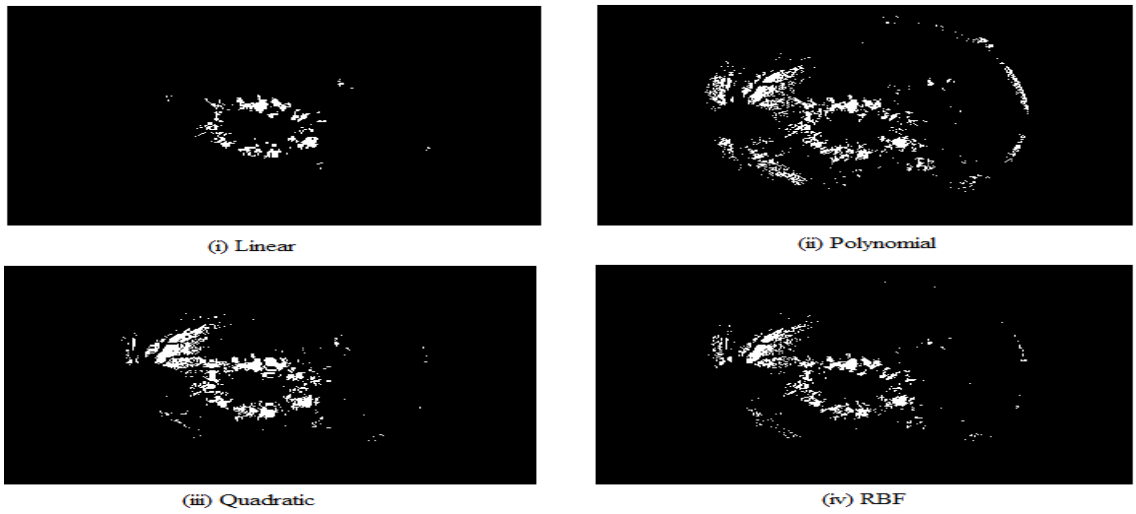

Figure-12. Black and white masking image of Figure-1(i) with varied kernel functions.

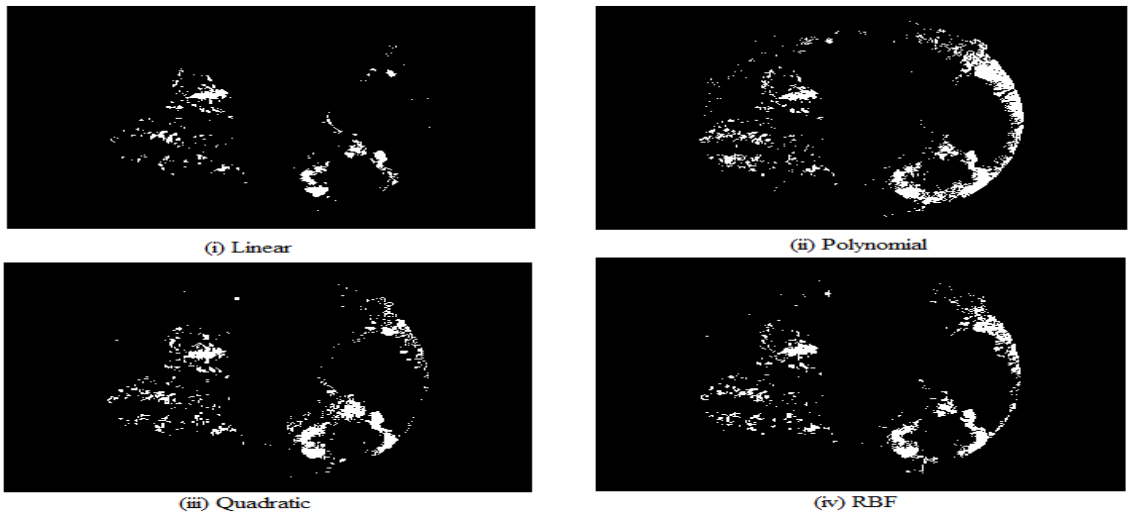

Figure-13. Black and white masking image of Figure-1(ii) with varied kernel functions.

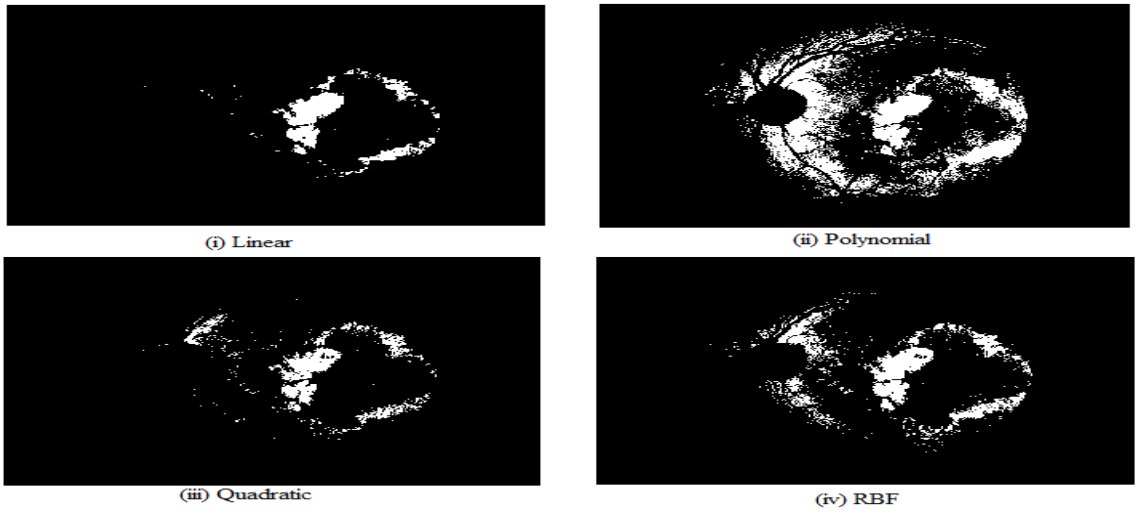

Figure-14. Black and white masking image of Figure-1(iii) with varied kernel functions.

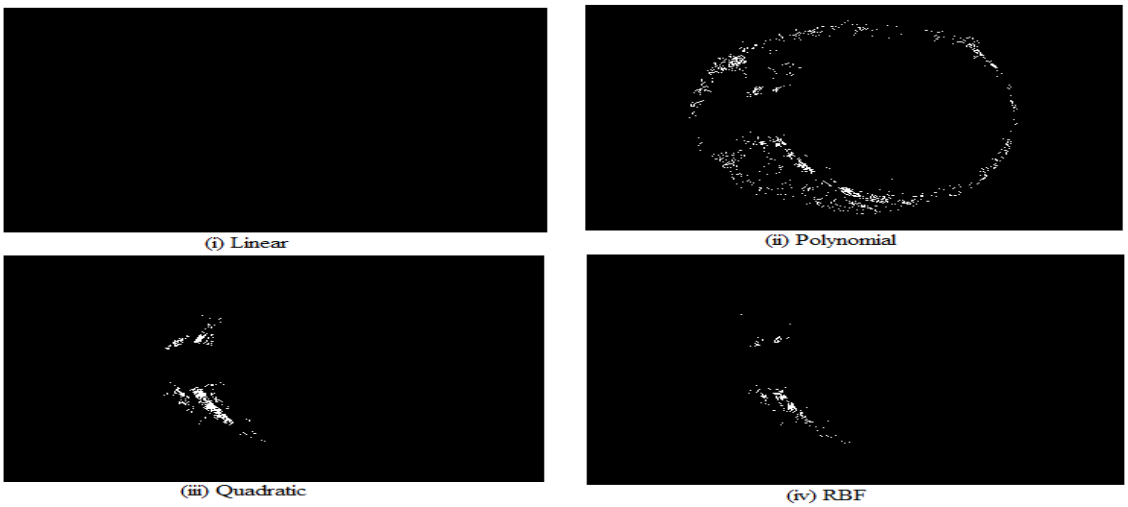

Figure-15. Black and white masking image of Figure-1 (iv) with varied kernel functions.

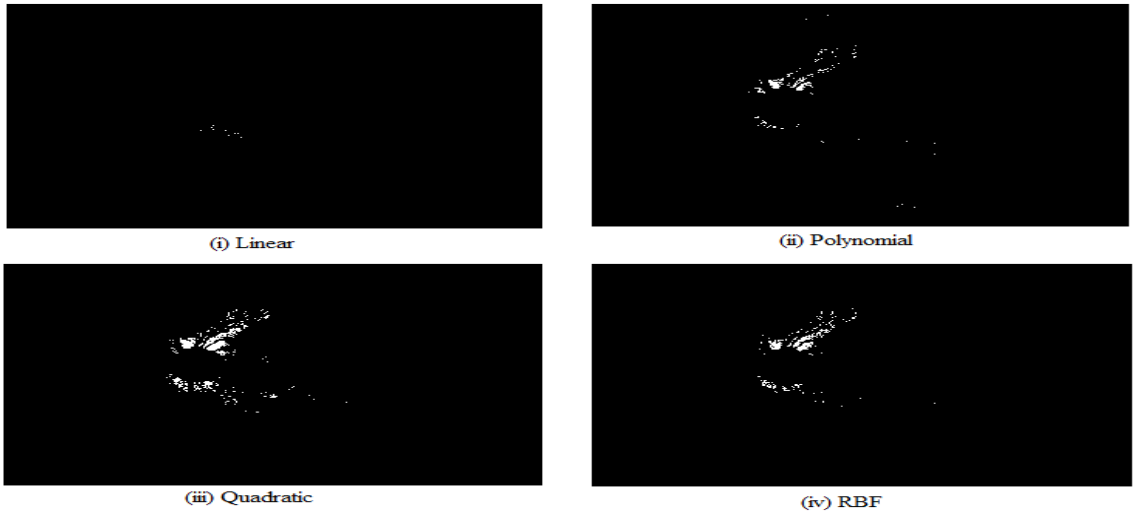

Figure-16. Black and white masking image of Figure-1(v) with varied kernel functions.

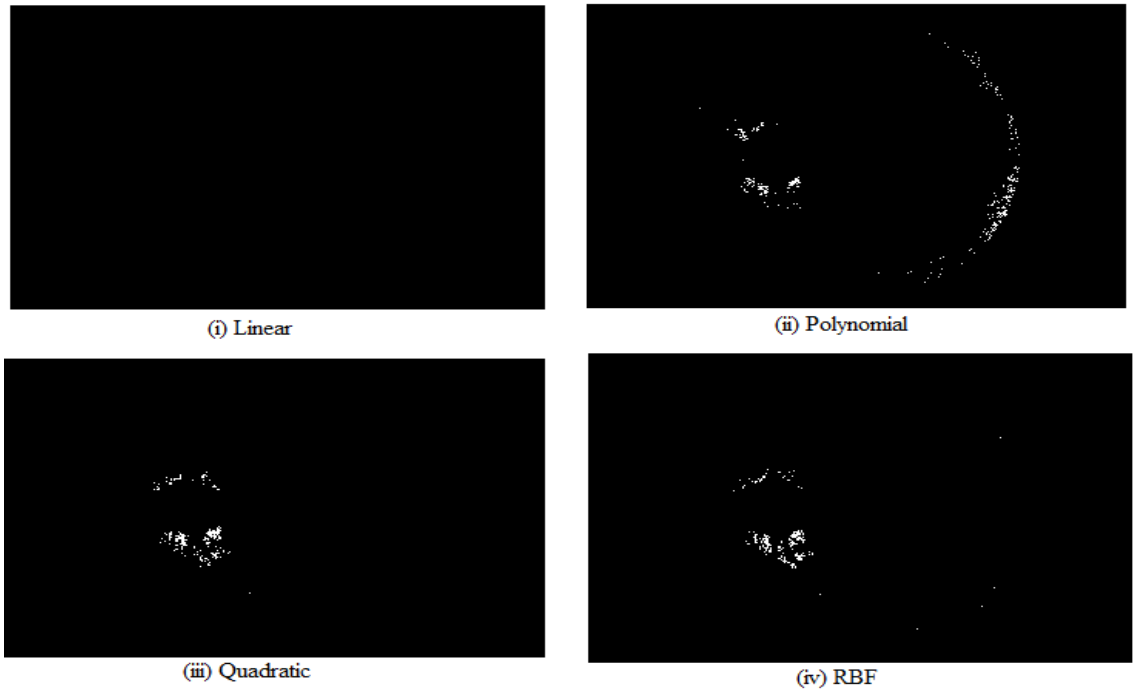

Figure-17. Black and white masking image of Figure-1(vi) with varied kernel functions.

CAC Implementation

A sample of exudates extracted from I_{wod} is shown in Figure-18. Here, two images were extracted using the CAC technique. The first image with removed OD (I_{wod})is shown in Figure-18(i). The grayscale conversion of $I_{wl}$is shown in Figure-18 (ii). Next, the areas marked as exudates were then subtracted from $I_{wod,}$which resulting an image with the exudates areas removed I_{wl} as shownin Figure-18 (iii). Then, the second image is I_{wl} masked on top of the I_{wod} image as shown in Figure-18 (iv).

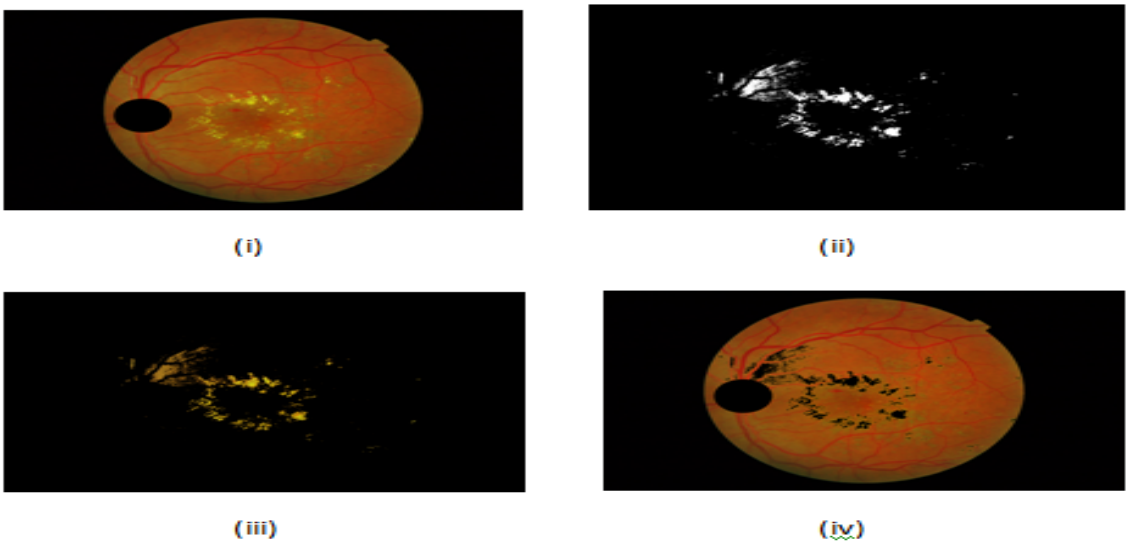

Figure-18. Exudates fundus image: i) I_{wod} fundus image, ii) I_{wl} grayscale fundus image, iii) I_{wl} color fundus image and iv) I_{wl} is masked on top of I_{wod} image.

Meanwhile, Figure-19 shows the result of the proposed algorithm application on a normal fundus image. The I_{wod} image is shown in Figure-19(i), and the result of I_{wl} grayscale conversion is shown in Figure-19 (ii). Relative to Figure-19(iii), Figure-19 (iii) shows that no areas were marked as exudates thus preserving the original image after the masking process (Figure-19 (iv)).

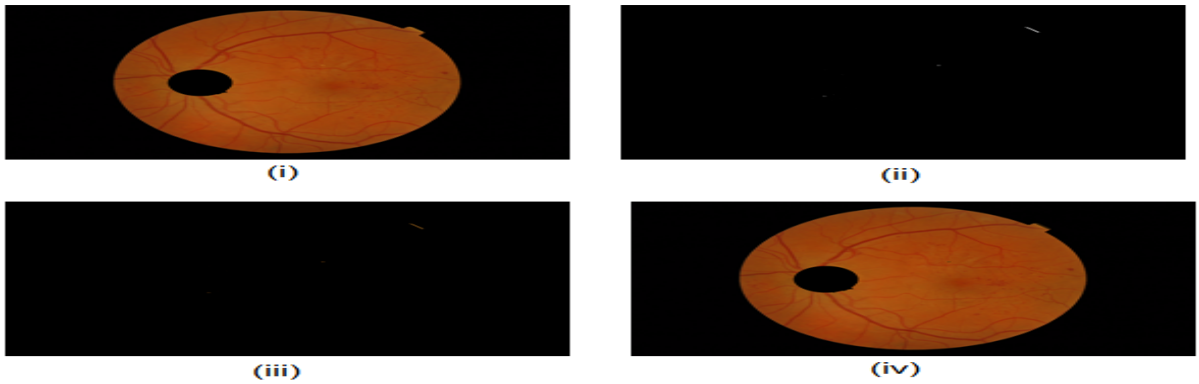

Figure-19. Normal fundus image: i) I_{wod} fundus image, ii) I_{wl} grayscale fundus image, iii) I_{wl} color fundus image and iv) I_{wl} is masked on top of I_{wod} image.

Classification of CAC features using MLP2

The MLP2 classifier was applied to diagnose DR based on CAC features. A summary of classification results for MLP2is shown in Table-5. For MLP2, even though hidden unit 2, 4, 8 and 10 show perfect classification accuracy in Table-5, they did not manage to effectively classify the CAC features well. It was observed that the best parameter in classifying accuracy is hidden unit 6 because the classification accuracy for both training and testing are 90.5% and 81.8% respectively. The overall accuracy of MLP2 for the optimal hidden units (6) on the training and testing sets were 90.5 and 81.8% respectively (Figure-20).

Table-5. MLP2 hidden unit and CAC features classification.

Hidden Unit	Classification Accuracy (%)
2	Training =89.5% Testing = 77.3%
4	Training = 82.9% Testing = 63.6%
6	Training = 90.5% Testing = 81.8%
8	Training = 85.7% Testing = 72.7%
10	Training = 85.7% Testing = 72.7%

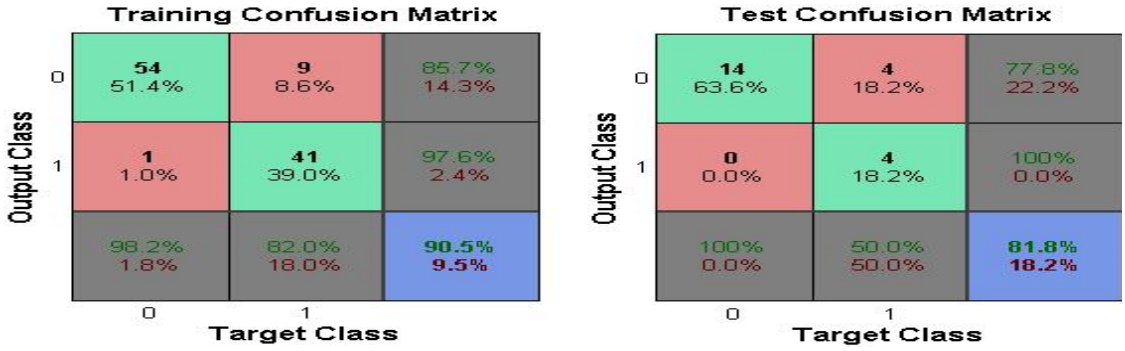

Figure-20. Confusion matrix for MLP2 (6 hidden units).

SVM2 classification

A summary of classification results for SVM2 is shown in Table-6.It was observed that, the best parameter in classifying accuracy is RBF kernel function because the classification accuracy for both training and testing were 93.3% and 83.8% respectively. Overall, 93.3% of the predictions are correct and 6.7% are wrong classifications for training. Meanwhile, for overall SVM testing shown in Figure-21, 83.8% of the predictions are correct and 16.2% are wrong classifications.

Table-6.SVM2 kernel function and CAC features classification.

Kernel Function	Classification Accuracy (%)
Linear	Training = 96.01% Testing = 81.1%
Polynomial	Training = 97.3% Testing = 70.3%
Quadratic	Training = 94.7% Testing = 64.9%
RBF	Training = 93.3% Testing = 83.8%

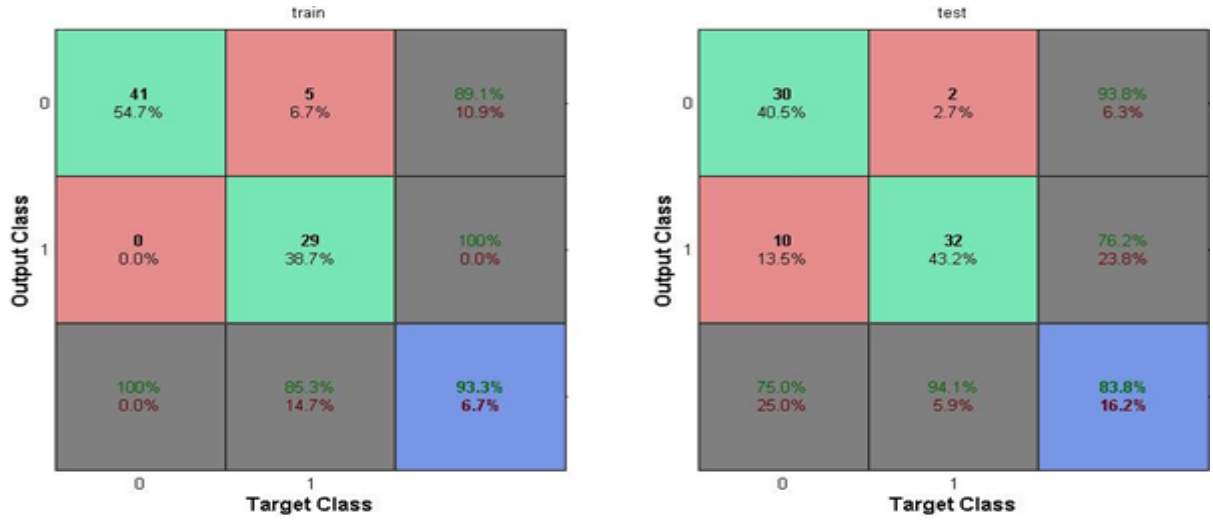

Figure-21. Confusion matrix for RBF kernel function.

CONCLUSIONS

This paper has demonstrated the ability of two types of classifiers (MLP and SVM) for 1) discrimination between exudate and non-exudate pixels in a fundus image, and 2) Diagnosis of DR based on CAC features. The results showed excellent discrimination ability of the classifiers (above 80%) under optimal parameters.

REFERENCES

[1] U.R.Acharya, C.M. Lim, E. Y. Ng, C. Chee and T. Tamura. 2009. Computer-based detection of diabetes retinopathy stages using digital fundus images. Proceedings of the Institution of Mechanical Engineers, Part H: Journal of Engineering in Medicine. 223(5): 545-553.

[2] International Diabetes Federation. 2015. Diabetes in Malaysia. http://www.idf.org/membership/wp/malaysia.

[3] Kovács L., Kurtán B., Eigner G., RudasI. and Chui C. K. 2015. Analysis of a novel time-delay diabetes model. In: IEEE European Control Conference.pp. 13-18.

[4] Rahaman S. 2012. Diabetes diagnosis decision support system based on symptoms, signs and risk factor using special computational algorithm by rule base. In: IEEE 15th International Conference on Computer and Information Technology.pp. 65-71.

[5] Hashim M.F. and HashimS.Z.M.2014. Diabetic retinopathy lesion detection using region-based approach. In: IEEE 8th Malaysian Software Engineering Conference.pp. 306-310.

[6] Sae-Tang W., ChiracharitW. and Kumwilaisak W. 2010. Exudates detection in fundus image using non-uniform illumination background subtraction. In: IEEE Region 10 Conference TENCON 2010.pp. 204-209.

[7] Gadriye D. and Khandale G. 2014. Neural network based method for the diagnosis of diabetic retinopathy. In: IEEE International Conference on Computational Intelligence and Communication Networks.pp. 1073-1077.

[8] K.K. Maheshand S.K. Nilesh. 2013. Review on fundus image acquisition techniques with data base reference to retinal abnormalities in diabetic retinopathy. International Journal of Computer Applications. 68(8): 17-27.

[9] K. Udayakumar, P.P. Bharati, S. Verma and M.K. Nath. 2015. Automatic estimation of vision degradation from color fundus image. International Journal of Image, Graphics and Signal Processing. 7(11): 26-34.

[10] LimS. T., ZakiW. M. D. W., Hussain A., LimS. L. and Kusalavan S.2011. Automatic classification of diabetic macular edema in digital fundus images. In: IEEE Colloquium on Humanities, Science and Engineering.pp. 265-269.

[11] L. Giancardo, F. Meriaudeau, T.P. Karnowski, Y. Li, S. Garg, K. W. Tobin and E. Chaum. 2012. Exudate-based diabetic macular edema detection in fundus images using publicly available datasets. Medical Image Analysis. 16(1): 216-226.

[12] S. Kavitha and K. Duraiswamy.2011. Automatic detection of hard and soft exudates in fundus images using color histogram thresholding.European Journal of Scientific Research. 48(3): 493-504.

[13] Zeljković V., Bojic M.,Tameze C. and Valev V. 2012. Classification algorithm of retina images of diabetic patients based on exudates detection. In:IEEE International Conference on High Performance Computing and Simulation.pp. 167-173.

[14] Oloumi F., Rangayyan R. M. and Ells A. L.2012. A graphical user interface for measurement of temporal arcade angles in fundus images of the retina. In: 25th IEEE Canadian Conference on Electrical and Computer Engineering. pp. 1-4.

[15] Mir H., Al-Nashash H. and Acharya U. R.2011. Assessment of retinopathy severity using digital fundus images. In: 1st Middle East Conference on Biomedical Engineering. pp. 200-203.

[16] Akram M.U., Nasir S., AnjumM. A. and JavedM. Y. 2009. Background and noise extraction from colored retinal images. In:IEEE WRI World Congress on Computer Science and Information Engineering.pp. 573-577.

[17] Purnama I.K.E. and AryantoK. Y. E. 2009. Branches filtering approach to extract retinal blood vessels in fundus image. In: International Conference on IEEE Instrumentation, Communications, Information Technology, and Biomedical Engineering. pp. 1-5.

[18] S. S.Basha and K. S. Prasad. 2008. Automatic detection of hard exudates in diabetic retinopathy using morphological segmentation and fuzzy logic. International Journal of Computer Science and Network Security. 8 (12): 211-218.

[19] M. D.Abràmoff, M.K. Garvin and M. Sonka. 2010. Retinal imaging and image analysis. IEEE Reviews in Biomedical Engineering.3: 169-208.

[20] M. Esmaeili, H. Rabbani, A.M. Dehnavi and A. Dehghani.2012. Automatic detection of exudates and optic disk in retinal images using curvelet transform. IET Image Processing .6 (7): 1005-1013.

[21] N. G.Ranamuka and R.G. N. Meegama. 2013. Detection of hard exudates from diabetic retinopathy images using fuzzy logic. IET Image Processing. 7 (2): 121-130.

[22] O. Faust, R. Acharya, E.Y.K. Ng, K.H. Ng and J. S. Suri. 2012. Algorithms for the automated detection of diabetic retinopathy using digital fundus images: A review. Journal of Medical Systems. 36 (1): 145-157.

[23] Singh A., Sengar N., DuttaM.K ., Riha K. and Minar J. 2015. Automatic exudates detection in fundus image using intensity thresholding and morphology. In:IEEE 7th International Congress on Ultra Modern Telecommunications and Control Systems and Workshops.pp. 330-334.

[24] PrincyeP. H. and Vijayakumari V. 2013. Detection of exudates and feature extraction of retinal images using fuzzy clustering method. In: IET Third International Conference on Computational Intelligence and Information Technology.pp. 388-394.

[25] G. Karegowda, A. Nasiha, M.A. Jayaram and A.S. Manjunath. 2011. Exudates detection in retinal images using back propagation neural network. International Journal of Computer Applications. 25(3): 25-31.

[26] Huang J. 1998. Color-spatial image indexing and applications.Phd thesis, Cornell University, New York, USA.

[27] Huang J. and Zabih R. 1998. Combiningcolor and spatial information for content-based image retrieval. In: 2nd European Conference on Research and Advanced Technology on Digital Libraries.

[28] Huang J., KumarS. R., Mitra M., Zhu W. J. and Zabih R.1997. Image indexing using color correlograms. In:IEEE Computer Society Conference on Computer Vision and Pattern Recognition.pp. 762-768.

[29] S. R. Singhand S. Kohli.2015. Enhanced CBIR using color moments, HSV histogram, color auto correlogram, and gabor texture. International Journal of Computer Systems. 2 (5): 161-165.

[30] Shen X., Wang X. and Du J. 2013. A novel image retrieval method based on color autocorrelogram and mutual information. In: International Conference on Advanced Computer Science and Electronics Information. pp. 587-590.

[31] Talib A., Mahmuddin M., Husni H. and George L. E. 2013. Efficient, compact, and dominant color correlogram descriptors for content-based image retrieval. In: 5th International Conferences on Advances in Multimedia. pp: 52-61.

[32] Mustaffa M.R., Ahmad F., Mahmod R. and Doraisamy S. 2012. Multi-resolution joint auto correlograms: determining the distance function. In: IEEE International Conference on Information Retrieval and Knowledge Management.pp. 198-202.

[33] Cai T.W., KimJ. and Feng D. D. 2008. Chapter 4: Content-based medical image retrieval.In: Biomedical Engineering: Biomedical Information Technology.D.D. Feng (Ed.).pp.83-113.

[34] A.Singla and M. Garg. 2014. CBIR approach based on combined hsv, auto correlogram, color moments and gabor wavelet. International Journal of

Engineering and Computer Science.3 (10): 9007-9012.

[35] Venkatesan R., Chandakkar P., Li B. and Li H. K. 2012. Classification of diabetic retinopathy images using multi-class multiple-instance learning based on color correlogram features. In: Annual International Conference of the IEEE Engineering in Medicine and Biology Society. pp. 1462-1465.

[36] ADCIS. 2016. MESSIDOR: Methods to evaluate segmentation and indexing techniques in the field of retinal opthalmology. http://www.adcis.net/en/Download-Third-Party/Messidor.html.

[37] Hassan H.A., Tahir N. M., Yassin I., Zabidi A., Yahaya C. C. and Shafie S. M. 2013. Automated optic disc removal in fundus images using iterative heuristics and morphological operations. In: IEEE Conference on Systems, Process and Control. pp. 230-233.

[38] A. H. A. R. Youssif, A.Z. Ghalwash and A.A.S.A.R. Ghoneim. 2008. Optic disc detection from normalized digital fundus images by means of a vessels' direction matched filter. IEEE Transactions on Medical Imaging. 27 (1): 11-18.

[39] MathWorks. 2015. Choose a multilayer neural network training function. http://www.mathworks.com/help/nnet/ug/choose-a-multilayer-neural-network-training-function.html.

[40] R. Sahak, W. Mansor, K.Y. Lee, A. Zabidi and A.I. Yassin. 2013. Optimization of principal component analysis and support vector machine for the recognition of infant cry with asphyxia. International Journal of Computers and Applications. 35 (3): 99-107.